ACI STRUCTURAL JOURNAL TECHNICAL PAPER

Title no. 110-S01

Ultimate Strength Domain of Reinforced Concrete Sections under Biaxial Bending and Axial Load

by Francesco Vinciprova and Giuseppe Oliveto

A direct method is provided for the construction of the ultimate strength domain of reinforced and/or prestressed concrete sections under biaxial bending and axial force. The method, based on the principle of plane sections, only requires the specification of the stress-strain relationships for each component material, the pretension strains, and possibly any other applied distortion. The results may be used for safety checks in new designs and in the rehabilitation of vulnerable or deteriorated structures. A few examples are used to demonstrate the performance of the method and its usefulness in practical applications.

Keywords: analytical techniques; biaxial bending; reinforced concrete sections; strength domain.

INTRODUCTION

The construction of the strength domains of cross sections of structural members has a long history. It is related to the problem of designing safe structures and is in fact to some degree an extension to the cross section of the strength criteria for materials such as Rankine, Tresca, and the Von Mises criteria, to quote only a few of the most popular. However, as is well-known, the strength criteria are often not in agreement with each other and some work is better than others, depending on the situation considered. Strength domains or failure surfaces in terms of stress resultants for a cross section should be the natural extension of strength criteria for materials. As there are six independent stress components for the Cauchy stress tensor, there are six stress resultants to be considered for the cross section—that is, an axial force, two shear forces, two bending moments, and a torque.

The task of producing a complete yield or resistance or rupture surface for a cross section is so daunting, however, that so far, none actually exist, even though in several branches of mechanics they are very much needed. The first complication with respect to a strength criterion is that there is the need for integration of the stress components over the cross section and the result is obviously dependent on the shape of the cross section. Moreover, the cross section is often of a composite nature, where different materials are used, such as concrete, reinforcing steel, prestressing steel, and fiber-reinforced polymer (FRP), to mention only widely used materials and technologies.

Although the six-dimensional domain is difficult to obtain exactly, several cross sections of the actual surface have been obtained with the development in the last century of metal and concrete structural plasticity. The results are available in textbooks on steel structures and on concrete structures.[1-3] Well-known, for instance, are the bending-moment-axial-force-interaction domains that are plane curves if the bending is direct. Even when neglecting both shear forces and torque, it has been recognized that in many instances the interaction of biaxial bending and axial force cannot be ignored. This has been recognized by most design codes in the world, which provide simplified methods to account for the abovementioned interaction. Among these are ACI 318,[4] AS 3600,[5] Eurocode 2 (EN 1992-1-1),[6] Eurocode 4 (EN-1994-1-1),[7] and Eurocode 8 (EN 1998-3).[8] In this paper, the authors are concerned with the development of a simple numerical algorithm for the construction of the interaction domain of reinforced concrete sections, possibly prestressed and/or including FRP in the form of bars or plies, or of steel sections encased in concrete or even tubular steel and FRP sections filled with concrete.

An overview of the state of the art in the field may be found in the paper by Furlong et al.[9] In this paper, only essential literature will be reviewed. All code developments are supported by scientific research and for the problem being considered, the relevant research is provided in a paper by Bresler,[10] where two empirical methods for the construction of the interaction surface are introduced—namely, the reciprocal load method (RLM) and the load contour method (LCM). Because these methods are well-known and available in the literature, it suffices to say that these are semi-analytical methods in the sense that they provide equations that, on the basis of empirically evaluated parameters, allow for the construction of the interaction surface.

Following this seminal paper, three main research lines have been pursued to deepen understanding of this topic. One line has consisted of experimental research aimed at checking the assumptions on the basis of the two methods mentioned in the previous paragraph and at evaluating the accuracy that can be obtained. Noteworthy among this research is the work by Ramamurthy.[11] Another line of research has been aimed at providing more accurate analytical expressions for the construction of the failure surface. The works by Ferguson et al.,[12] Wight and Mac Gregor,[13] Silva et al.,[14] and Bonet et al.[15] follow this line. However, a considerable effort has been devoted to a third line of research, which has tackled the problem of providing the failure surface using numerical algorithms based on the integration of the governing equilibrium equations and constitutive laws for the constituent materials. Early basic work is considered in textbooks by Park and Pauley,[16] Nielsen,[17] and MacGregor and Bartlett.[18] Also in this line or research are the works by Kawakami et al.[19]; Landonio and Perego[20]; Hulse and Mosley[21]; Contaldo and Faella[22]; Spiegel and Limbrunner[23]; Bousias et al.[24]; De Vivo and Rosati[25]; Rodriguez-Gutierrez and Aristizabal-Ochoa[26]; Rodriguez-Gutierrez and Aristizabal-Ochoa,[27] who also considered prestressed concrete

ACI Structural Journal, V. 110, No. 1, January-February 2013.

Francesco Vinciprova *is a Lecturer of physics and mathematics at the Bonaventura Secusio High School, Caltagirone, Sicily, Italy. He received his MS in civil engineering and his PhD in structural engineering at the University of Catania, Sicily, Italy. His research interests include the field of application of boundary element methods in structural mechanics and structural dynamics.*

Giuseppe Oliveto *is Full Professor of structural engineering at the University of Catania. His research interests include the structural mechanics, structural dynamics, and earthquake engineering.*

sections; Fafitis,[28] who transforms the double equilibrium integrals into line integrals; Sfakianakis[29]; Consolazio et al.[30]; Hock and Cheong[31]; Charalampakis and Koumousis[32]; and Di Ludovico et al.[33] Other works in this line study the integration methods of the stresses over the cross section. Among these are studies by Bonet et al.[34,35]

The reference by Di Ludovico et al.[33] is notable for a state-of-the-art treatment of the topic and because it provides a good basis for the work that will be presented herein. The paper develops a numerical algorithm based on a finite element discretization of the cross section. The applied load is increased monotonically until the ultimate limit state of the cross section is reached. For a given value of the axial force acting on the cross section, the loading axis in the cross section is provided. For a given value of the bending moment, which is perpendicular to the loading axis, a nonlinear system of equations must be solved to find the position of the neutral axis and subsequently strains, stresses, and stress resultants. This procedure is iterated several times for successive increments of the bending moment or curvature until the ultimate limit state for the cross section is reached. Having completed this task, one point of the failure surface of the cross section under axial force and biaxial bending is found. Other points are obtained by slightly changing the ratio between bending moments and repeating the previous task. In the end, a cross section of the failure surface for constant axial force is generated.

RESEARCH SIGNIFICANCE

The construction of the entire failure surface with the method described at the end of the introduction requires the repetition of the previously described tasks for several values of the axial force, from the failure value in compression to the failure value in tension. It is obvious that the construction of the entire failure surface in this way is a very time-consuming task, but a much more efficient method is available. This method, already known in literature and recommended by Marín[36] but somewhat neglected, will be formulated and exploited in the following sections.

GENERAL FORMULATION OF THE PROBLEM

Given a cross section of general shape and material composition (Fig. 1), the problem is to solve is the construction of the failure surface under axial force and biaxial bending in the quickest way possible. To make the problem as general as possible, assume that the cross section does not admit axes of symmetry. Let a Cartesian orthogonal reference frame O, X, Y be defined within the plane of the cross section, to which the axial force and the bending moments are referred. For a given position of the neutral axis, a rotated Cartesian orthogonal reference system O, x, y is defined such that the x-axis is parallel to the neutral axis n, and α is the anti-clockwise rotation of the x-axis with respect to the X-axis. The Bernoulli hypothesis, which states that initially plane cross sections remain plane after deformation, allows for the deformation shown graphically in Fig. 1 to be given by the following mathematical expression

$$\varepsilon = \varepsilon_0 + \kappa y \tag{1}$$

where ε_0 is the axial strain on the fiber defined by the equation $y = 0$; and κ is the curvature.

At this point, one can only assume that the axial stress is related to the axial strain via a general nonlinear relation-

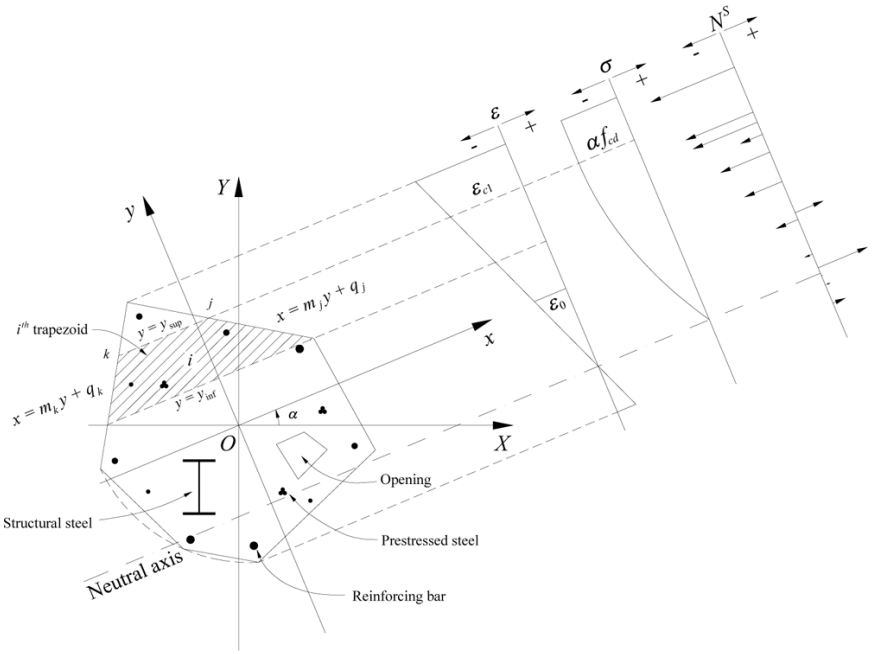

Fig. 1—General cross section, global and local reference frames, neutral axis, and strain and stress diagrams.

ship—that is, $\sigma = f(\varepsilon)$—where only one value of the stress corresponds to a given value of the strain, while more than one strain may correspond to a given stress.

The three equations given as follows must be satisfied to ensure equilibrium between internal stresses and externally applied load resultants

$$\begin{aligned}\int_A \sigma dA &= \int_A f(\varepsilon)\, dA = N \\ \int_A y\sigma dA &= \int_A yf(\varepsilon)\, dA = M_x \\ \int_A x\sigma dA &= \int_A xf(\varepsilon)\, dA = M_y\end{aligned} \tag{2}$$

The transformation of coordinates

$$\begin{bmatrix} x \\ y \end{bmatrix} = \begin{bmatrix} \cos\alpha & -\sin\alpha \\ \sin\alpha & \cos\alpha \end{bmatrix} \cdot \begin{bmatrix} X \\ Y \end{bmatrix} \tag{3}$$

allows for Eq. (2) to be written with reference to the fixed reference frame O, X, Y, providing the following system of equations

$$\begin{aligned}&\int_A f(\varepsilon)\, dA = N \\ &\sin\alpha \int_A X \cdot f(\varepsilon)\, dA + \cos\alpha \int_A Y \cdot f(\varepsilon)\, dA = M_X \cos\alpha - M_Y \sin\alpha \\ &\cos\alpha \int_A X \cdot f(\varepsilon) \cdot dA - \sin\alpha \int_A Y \cdot f(\varepsilon) \cdot dA = M_X \sin\alpha + M_Y \cos\alpha\end{aligned} \tag{4}$$

The system of Eq. (4) provides the proper basis for the problem. In most of the literature, the problem is approached in the following way. Given the three stress resultants (N, M_X, M_Y), find the position of the neutral axis—that is, the angle α and the ordinate $y_0 = \varepsilon_0/\kappa$—and check whether the ultimate strain has been exceeded in the most distant fibers from the neutral axis. Generally, a loading process is assigned by which the external stress resultants are increased step by step according to a given law until a failure condition is reached—that is, one of the component materials in the cross section reaches the rupture strain. It is evident that the governing system of equations is highly nonlinear because of the nonlinearity of the constitutive laws of the constituent materials and because of the geometrical nonlinearity associated to the position of the neutral axis. This system must be solved many times just to obtain a single point of the failure surface. It is obvious that this is not a very efficient method if one wants just to construct the failure surface of a given cross section. However, the method may be justified if one has just one set of stress resultants and wants to check whether this is safe or not, or what the safety coefficient is for a given loading path.

Before a much more efficient method of producing the failure surface is formulated, it may be worth noting that the given system of Eq. (4) is strictly sufficient for the evaluation of the three kinematical unknowns α, ε_0, and κ, which solve the problem.

MARÍN'S METHOD

The following describes a much more efficient way of solving the problem of constructing the failure surface of a cross section under axial force and biaxial bending. Although the method has often been used by engineers to solve problems elegantly that otherwise would be very hard to solve, it was recommended in the present context by Marín[36] in 1979 to satisfy the ACI 318-71 requirements. Rather than starting from a set of stress resultants and then trying to find a point of the failure surface by following a given step-by-step loading process, the method starts from a given position of the neutral axis—that is, angle α and the equation of the neutral axis are known

$$y = y_0 \tag{5}$$

Equation (1) and Eq. (5) provide the following results

$$\varepsilon_0 = -\kappa \cdot y_0 \qquad \varepsilon = \kappa \cdot (y - y_0) \tag{6}$$

For each material that constitutes the cross section, the maximum strain ε_i is related to the maximum distance y_i from the neutral axis via the relationship

$$\varepsilon_i = \kappa \cdot (y_i - y_0) \qquad i = 1, 2, \ldots, N \tag{7}$$

The failure of the cross section occurs as soon as a material reaches the rupture or breaking strain—namely $\varepsilon_f = \varepsilon_f^r$—and the curvature that leads the cross section to failure, for the given position of the neutral axis, is given by the equation

$$\kappa_r = \frac{\varepsilon_j^r}{y_j - y_0} \tag{8}$$

At this point, the strain diagram at failure is completely known if the result from Eq. (8) is used in Eq. (6). The corresponding stress resultants may be obtained by using Eq. (2), while a coordinate transformation provides the results in the fixed coordinate system O, X, Y. The set of stress resultants thus evaluated provides a point of the failure surface of the cross section. The most important thing that must be observed is that there are no nonlinear equations to be solved with this method and the only operations needed are the integral calculations for the evaluation of the stress resultants. As will be shown later, even those can be performed in closed form.

The construction of the failure surface proceeds with the calculation of a family of isogonic lines, each of them associated with a given angle α for the neutral axis. By translating the neutral axis slowly, a set of failure points on a isogonic line may be generated. These points may be as close as one wishes because their distance depends only on the amount by which the neutral axis is translated. The isogonic lines are not generally plane curves, but are certainly plane if the neutral axis is parallel to one of the principal axes of the cross section. Once an isogonic line has been completed, the next one is constructed by rotating the neutral axis by a convenient amount. It is obvious that the family of isogonic lines thus constructed allows for a complete characterization of the failure surface of a given cross section. The whole surface may be constructed or simply areas of the entire surface of specific interest. The accuracy of the whole surface or of a required area can be made as good as required by reducing the translation and rotational steps of the neutral axis.

IMPLEMENTATION OF METHOD

The implementation of the model requires some basic operations that are listed in the following. The first step is the descrip-

tion of the cross section with the definition of exterior and interior boundaries, position of reinforcement and pretensioned bars, position of FRP bars and/or plies, and position of structural steel. The second step consists of the definition of the constitutive laws of the constituent materials. The third step consists of the calculation of the stress resultants as specified by Eq. (2) and the final step consists of their transformation into the fixed reference frame *O*, *X*, *Y*. The various phases that have been listed previously will be described in some detail as follows.

Description of cross section

It is assumed that all boundaries of the cross section are straight line segments; if a curved boundary exists, it is assumed that this can be approximated by a polygonal, which can be made as close as possible to the given boundary as the number of vertices of the approximating polygonal increases. All geometrical parameters are referred to the fixed reference frame *O*, *X*, *Y* as follows:

- X_i^c and Y_i^c are the coordinates of the vertices of the various boundaries of the cross section;
- X_i^s and Y_i^s are the coordinates of the centroid of the ordinary reinforcing bars;
- X_i^{sp} and Y_i^{sp} are the coordinates of the centroid of the prestressing bars; and
- X_i^{ss} and Y_i^{ss} are the coordinates of the vertices of the structural steel section encased in the concrete section.

The corresponding coordinates in the local reference frame *O*, *x*, *y* are obtained via the coordinate transformation provided by Eq. (3). The equation of the boundary segment *j* between vertices *i* and *i* + 1 takes the expression

$$x = m_j y + q_j \tag{9}$$

where

$$m_j = \frac{x_{i+1}^C - x_i^C}{y_{i+1}^C - y_i^C} \qquad q_j = x_i^C - \frac{x_{i+1}^C - x_i^C}{y_{i+1}^C - y_i^C} y_i^C \tag{10}$$

provided that the segment is not parallel to the *x*-axis, in which case the equation becomes

$$y = y_i^C = y_{i+1}^C \tag{11}$$

Constitutive laws

Any of the constitutive laws used in the literature are allowed within the context of this work; for instance, the constitutive laws listed by Di Ludovico et al.[33] However, for illustrative purposes, some constitutive laws recommended by Eurocode 2[6] and Eurocode 4[7] are used herein, along with the softening Kent and Park[37] law for unconfined concrete.

According to the considered Eurocodes, the constitutive law for concrete assumes that the concrete does not respond in tension while a parabola-rectangle stress diagram is associated to compression strains. In mathematical terms, this may be expressed as follows

$$\begin{aligned}
&\sigma_c(\varepsilon) = 0 && \forall \varepsilon \geq 0 \\
&\sigma_c(\varepsilon) = -\alpha \cdot f_{cd} \frac{\varepsilon}{\varepsilon_{c1}}\left(2 - \frac{\varepsilon}{\varepsilon_{c1}}\right) && \forall \varepsilon \in [\varepsilon_{c1}, 0] \\
&\sigma_c(\varepsilon) = -\alpha \cdot f_{cd} && \forall \varepsilon \in [\varepsilon_{cu}, \varepsilon_{c1}]
\end{aligned} \tag{12}$$

When the Kent and Park[37] law is used, the first and second equations of Eq. (12) still hold while the third equation is replaced by Eq. (13), with stress varying linearly from $-\alpha \cdot f_{cd}$ to $-\beta \cdot f_{cd}$.

$$\sigma(\varepsilon) = \left[-\alpha + \frac{\varepsilon - \varepsilon_{c1}}{\varepsilon_{cu} - \varepsilon_{c1}}(\alpha - \beta)\right] f_{cd} \quad \forall \varepsilon \in [\varepsilon_{cu}, \varepsilon_{c1}] \tag{13}$$

By setting

$$t_0 = \frac{\varepsilon_0}{\varepsilon_{c1}}\left(2 - \frac{\varepsilon_0}{\varepsilon_{c1}}\right) \quad t_1 = \frac{2\kappa}{\varepsilon_{c1}}\left(1 - \frac{\varepsilon_0}{\varepsilon_{c1}}\right) \quad t_2 = -\frac{\kappa^2}{\varepsilon_{c1}^2} \tag{14}$$

the second equation of Eq. (12) may be written as follows

$$\sigma_c(y) = -\alpha \cdot f_{cd}\left(t_0 + t_1 y + t_2 y^2\right) \tag{15}$$

By setting

$$t_0^L = \frac{\left(\frac{\beta}{\alpha} - 1\right)\varepsilon_0 - \frac{\beta}{\alpha}\varepsilon_{c1} + \varepsilon_{cu}}{\varepsilon_{cu} - \varepsilon_{c1}} \qquad t_1^L = \frac{\kappa\left(\frac{\beta}{\alpha} - 1\right)}{\varepsilon_{cu} - \varepsilon_{c1}} \tag{16}$$

Equation (13) may be written as follows

$$\sigma_c(y) = -\alpha \cdot f_{cd}\left(t_0^L + t_1^L y\right) \tag{17}$$

The parameters appearing in the previous equations are specified by Eurocodes 2 and 4.

The constitutive law for reinforcing steel assumes elastic-perfectly plastic behavior with limited tensile and compression strain. In mathematical terms, this is expressed by the following equations

$$\begin{aligned}
&\sigma_s(\varepsilon) = E_s \varepsilon && \forall \varepsilon \in [-\varepsilon_{yd}, \varepsilon_{yd}] \\
&\sigma_s(\varepsilon) = \operatorname{sgn}(\varepsilon) E_s \varepsilon_{yd} && \forall \varepsilon \in [-\varepsilon_{su}, -\varepsilon_{yd}] \cup [\varepsilon_{yd}, \varepsilon_{su}]
\end{aligned} \tag{18}$$

For prestressing steel, Eurocode 2 specifies a bilinear stress-strain relationship

$$\begin{aligned}
&\sigma_p = f_{pd} \frac{\varepsilon}{\varepsilon_{yd}} && \forall \varepsilon \in [0, \varepsilon_{yd}] \\
&\sigma_p = f_{pd} + \left(\frac{f_{pk}}{\gamma_s} - f_{pd}\right)\frac{\varepsilon - \varepsilon_{yd}}{\varepsilon_{ud} - \varepsilon_{yd}} && \forall \varepsilon \in [\varepsilon_{yd}, \varepsilon_{ud}]
\end{aligned} \tag{19}$$

Stress resultants

The cross section is divided into a finite number of trapezoids with bases parallel to the neutral axis and the two oblique sides belonging to its boundary, as is shown in Fig. 1. The partition lines parallel to the neutral axis, besides the neutral axis itself defined by the equation $y = y_0$ and the straight line $y = y_{c1}$ for which it is $\varepsilon(y_{c1}) = \varepsilon_{c1}$, all pass through vertices of the boundary of the cross section. Axial force *N* and bending moments M_x and M_y may be given by the expressions

$$N = \sum_{i=1}^{n^S} N_i^S + \sum_{i=1}^{n^S_p} N_i^P + \sum_{i=1}^{n^{SS}} N_i^{SS} + \sum_{i=1}^{n_t^C} N_i^C + \sum_{i=1}^{n_{cP}^C} N_i^C + \sum_{i=1}^{n_{cL}^C} N_i^C + \sum_{i=1}^{n_{cR}^C} N_i^C$$
$$M_x = \sum_{i=1}^{n^S} M_{xi}^S + \sum_{i=1}^{n^S_p} M_{xi}^P + \sum_{i=1}^{n^{SS}} M_{xi}^{SS} + \sum_{i=1}^{n_t^C} M_{xi}^C + \sum_{i=1}^{n_{cP}^C} M_{xi}^C + \sum_{i=1}^{n_{cL}^C} M_{xi}^C + \sum_{i=1}^{n_{cR}^C} M_{xi}^C \quad (20)$$
$$M_y = \sum_{i=1}^{n^S} M_{yi}^S + \sum_{i=1}^{n^S_p} M_{yi}^P + \sum_{i=1}^{n^{SS}} M_{yi}^{SS} + \sum_{i=1}^{n_t^C} M_{yi}^C + \sum_{i=1}^{n_{cP}^C} M_{yi}^C + \sum_{i=1}^{n_{cL}^C} M_{yi}^C + \sum_{i=1}^{n_{cR}^C} M_{yi}^C$$

where n^S is the total number of ordinary reinforcing steel rods; n^S_p is the total number of pretensioned steel bars; n^{SS} is the number of trapezoids into which the structural steel is divided; n^C_t is the number of trapezoids into which the part of cross section in tension is divided; n^C_{cp} is the number of trapezoids in the compression part of the cross section where the stress has a parabolic distribution; n^C_{cL} is the number of trapezoids in the compression part of the cross section where the stress has a linear distribution; and n^C_{cR} is the number of trapezoids in the compression part of the cross section where the stress is constant.

Let us now consider the *i*-th trapezoid whose oblique sides are the *j*-th and the *k*-th sides of the polygon, which defines the boundary of the cross section, and let y_{sup} and y_{inf} be the ordinates of the two bases of the trapezoid.

The contributions to the stress resultants of the trapezoid considered are calculated as follows

$$N_i^C = \int_{y_{inf}}^{y_{sup}} \int_{x_k(y)}^{x_j(y)} \sigma_c(x,y)\,dxdy = \int_{y_{inf}}^{y_{sup}} \int_{m_k y+q_k}^{m_j y+q_j} \sigma_c(x,y)\,dxdy$$
$$M_{x_i}^C = \int_{y_{inf}}^{y_{sup}} \int_{x_k(y)}^{x_j(y)} \sigma_c(x,y)\,y\,dxdy = \int_{y_{inf}}^{y_{sup}} \int_{m_k y+q_k}^{m_j y+q_j} \sigma_c(x,y)\,y\,dxdy \quad (21)$$
$$M_{y_i}^C = \int_{y_{inf}}^{y_{sup}} \int_{x_k(y)}^{x_j(y)} \sigma_c(x,y)\,x\,dxdy = \int_{y_{inf}}^{y_{sup}} \int_{m_k y+q_k}^{m_j y+q_j} \sigma_c(x,y)\,x\,dxdy$$

By using Eq. (9), (11), (15), and (17), the aforementioned integrals lead to the following results if the trapezoid belongs to the region where the stress has a parabolic distribution

$$N_i^C = -\alpha f_{cd}\left\{t_0(q_j-q_k)(y_{sup}-y_{inf}) + \left[t_0(m_j-m_k)+t_1(q_j-q_k)\right]\frac{y_{sup}^2-y_{inf}^2}{2} + \left[t_1(m_j-m_k)+t_2(q_j-q_k)\right]\frac{y_{sup}^3-y_{inf}^3}{3} + t_2(m_j-m_k)\frac{y_{sup}^4-y_{inf}^4}{4}\right\}$$
$$M_{xi}^C = -\alpha f_{cd}\left\{t_0(q_j-q_k)\frac{y_{sup}^2-y_{inf}^2}{2} + \left[t_0(m_j-m_k)+t_1(q_j-q_k)\right]\frac{y_{sup}^3-y_{inf}^3}{3} + \left[t_1(m_j-m_k)+t_2(q_j-q_k)\right]\frac{y_{sup}^4-y_{inf}^4}{4} + t_2(m_j-m_k)\frac{y_{sup}^5-y_{inf}^5}{5}\right\} \quad (22)$$
$$M_{yi}^C = -\alpha f_{cd}\left\{\frac{1}{2}t_0(q_j^2-q_k^2)(y_{sup}-y_{inf}) + \left[t_0(m_jq_j-m_kq_k)+\frac{1}{2}t_1(q_j^2-q_k^2)\right]\frac{y_{sup}^2-y_{inf}^2}{2} + \left[\frac{1}{2}t_0(m_j^2-m_k^2)+t_1(m_jq_j-m_kq_k)+\frac{1}{2}t_2(q_j^2-q_k^2)\right]\frac{y_{sup}^3-y_{inf}^3}{3} + \left[\frac{1}{2}t_1(m_j^2-m_k^2)+t_2(m_jq_j-m_kq_k)\right]\frac{y_{sup}^4-y_{inf}^4}{4} + \frac{1}{2}t_2(m_j^2-m_k^2)\frac{y_{sup}^5-y_{inf}^5}{5}\right\}$$

If the trapezoid belongs to the region where the stress is linear, the following results are found

$$N_i^C = -\alpha f_{cd}\left\{t_0^L(q_j-q_k)(y_{sup}-y_{inf}) + \left[t_0^L(m_j-m_k)+t_1^L(q_j-q_k)\right]\frac{y_{sup}^2-y_{inf}^2}{2} + t_1^L(m_j-m_k)\frac{y_{sup}^3-y_{inf}^3}{3}\right\}$$
$$M_{xi}^C = -\alpha f_{cd}\left\{t_0^L(q_j-q_k)\frac{y_{sup}^2-y_{inf}^2}{2} + \left[t_0^L(m_j-m_k)+t_1^L(q_j-q_k)\right]\frac{y_{sup}^3-y_{inf}^3}{3} + t_1^L(m_j-m_k)\frac{y_{sup}^4-y_{inf}^4}{4}\right\}$$
$$M_{yi}^C = -\alpha f_{cd}\left\{\frac{1}{2}t_0^L(q_j^2-q_k^2)(y_{sup}-y_{inf}) + \left[t_0^L(m_jq_j-m_kq_k)+\frac{1}{2}t_1^L(q_j^2-q_k^2)\right]\frac{y_{sup}^2-y_{inf}^2}{2} + \left[\frac{1}{2}t_0^L(m_j^2-m_k^2)+t_1^L(m_jq_j-m_kq_k)\right]\frac{y_{sup}^3-y_{inf}^3}{3} + \frac{1}{2}t_1^L(m_j^2-m_k^2)\frac{y_{sup}^4-y_{inf}^4}{4}\right\} \quad (23)$$

If, instead, the trapezoid belongs to the region where the stress is constant, it results

$$N_i^C = -\alpha f_{cd}\left[(q_j-q_k)(y_{sup}-y_{inf}) + (m_j-m_k)\frac{y_{sup}^2-y_{inf}^2}{2}\right]$$
$$M_{xi}^C = -\alpha f_{cd}\left[(q_j-q_k)\frac{y_{sup}^2-y_{inf}^2}{2} + (m_j-m_k)\frac{y_{sup}^3-y_{inf}^3}{3}\right] \quad (24)$$
$$M_{yi}^C = -\alpha f_{cd}\left[\frac{1}{2}(q_j^2-q_k^2)(y_{sup}-y_{inf}) + (m_jq_j-m_kq_k)\frac{y_{sup}^2-y_{inf}^2}{2} + \frac{1}{2}(m_j^2-m_k^2)\frac{y_{sup}^3-y_{inf}^3}{3}\right]$$

Equations (22) through (24) provide closed-form contributions to the stress resultants and are only valid for the constitutive laws for concrete defined in the appropriate section above. However, corresponding results may be easily found for several other common constitutive laws.

EXAMPLES AND COMPARISON WITH RESULTS IN LITERATURE

In this section, results obtained using the presented method are compared with those available in the literature. The results are also compared to those obtained using fiber models, as implemented in the OpenSees[38] software. Problems, which may arise when using those methods or similar ones, are highlighted and the usefulness of the proposed method is reaffirmed. Strength domains for some typical cross sections are also shown.

Comparison of results for square cross section

The simplest cross section that can be considered is the rectangular one. Some results for this type of cross section are shown by Di Ludovico et al.[33] The 250 x 250 mm (9.84 x 9.84 in.) square cross section shown in Fig. 2 is provided with four reinforcement bars, each 12 mm (0.472 in.) in diameter, with a concrete cover of 30 mm (1.18 in.).

The material properties considered, also shown in Fig. 2, are steel design yield stress f_{yd} = 278 MPa (40.32 ksi) and concrete design strength αf_{cd} = 13.28 MPa (1.93 ksi).

The strength domain constructed by using the method presented in the previous section is shown in Fig. 3(a). In the construction of this domain, the rotation of the neutral axis from one position to the adjacent one was chosen as 10 degrees or π/18 radians. Therefore, 18 isogonic curves were generated. The number of points on each of these curves was established by requiring 25 points for each characteristic rupture mode of the cross section, defined by a strain interval $]\varepsilon_{min}, \varepsilon_{max}[$. Because there are six rupture modes, the total number of points on each isogonic curve turns out to be equal to 150. Therefore, the surface, or boundary, of the strength domain shown in Fig. 3 is identified by an irregular grid of 18 x 150 points. The quadrilaterals visible in Fig. 3 each correspond to two adjacent isogonic curves and two adjacent strain values.

The intersection of the strength domain with planes of constant axial force, as shown in Fig. 3(b), provides the

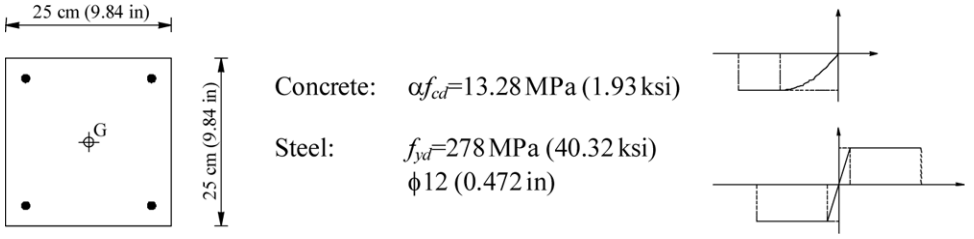

Fig. 2—Reinforced concrete square cross section considered by Di Ludovico et al.[33]

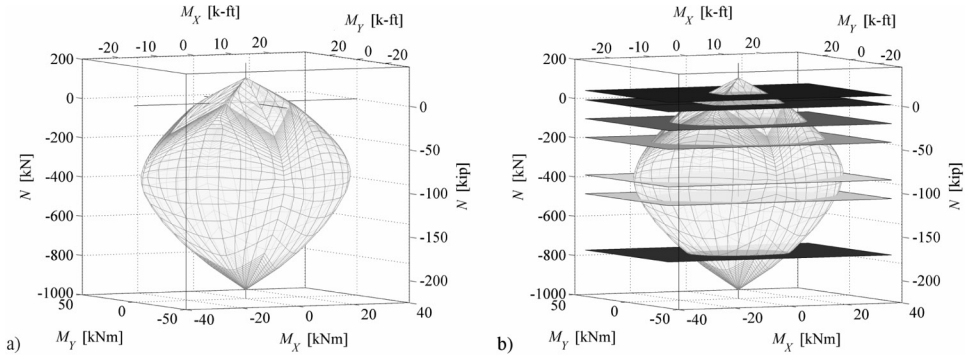

Fig. 3—Strength domain for reinforced concrete section shown in Fig. 2: (a) domain; and (b) planes of constant axial force.

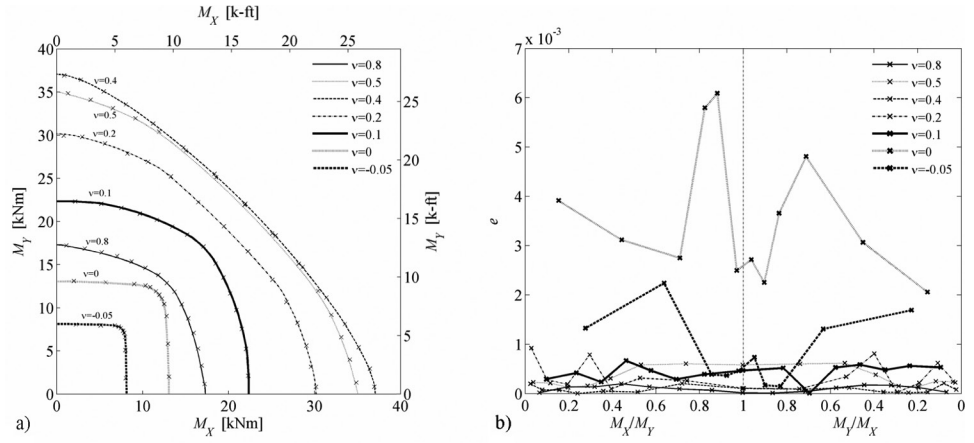

Fig. 4—Cross sections of strength domain for constant axial force: (a) comparison with results by Di Ludovico et al.[33]; and (b) relative error.

plane curves given in Fig. 4(a). These were produced to compare the results obtained by the presented method with corresponding results available in the literature. In fact, the results by Di Ludovico et al.[33] were given in the form of discrete points in the M_X-M_r plane, for various levels of axial force. In Fig. 4(a), the continuous lines refer to the results of the present method, while the symbols show the results by Di Ludovico et al.,[33] each line being characterized by a given ratio ν of the actual axial force to the ultimate value in compression. The agreement is excellent, showing that both methods lead to the same results. However, it should be noticed that no iterations are needed to produce the present results and the entire strength domain can be derived with little computational effort.

To have a quantitative measure of the accuracy of the results obtained and to be able to make a comparison with other methods, the following definition is adopted for the error. If $P - O$ is the vector denoting the solution obtained by the present method and $Q - O$ denotes the solution obtained by another method, the relative error may be defined by the following formula

$$e = \sqrt{\frac{(Q-P)\cdot(Q-P)}{(P-O)\cdot(P-O)}} \tag{25}$$

The graph of the error of the results provided by Di Ludovico et al.[33] is shown in Fig. 4(b). It may be seen that the maximum error is less than 0.01.

The software OpenSees (Mazzoni et al.[39]) has been used to implement a fiber model for the evaluation of some points

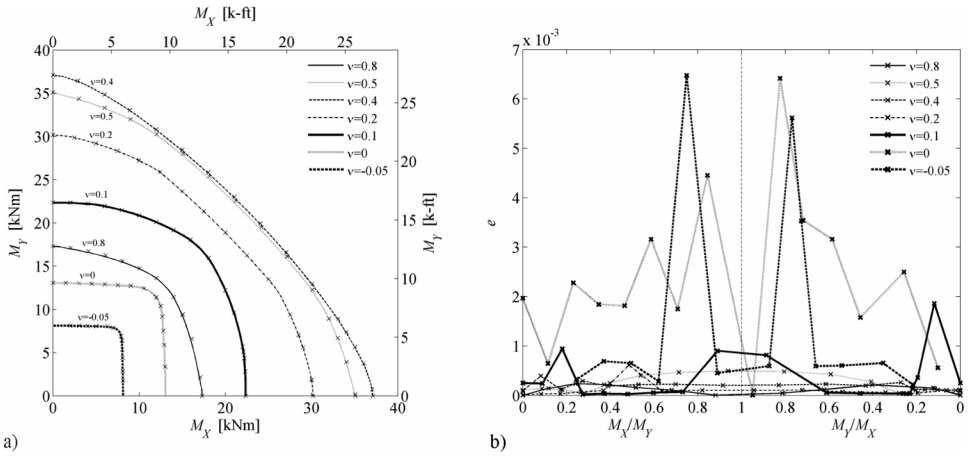

Fig. 5—Cross sections of strength domain for constant axial force: (a) comparison with results obtained by using OpenSees software, given values of axial force N *and of two curvatures; and (b) relative error.*

of the boundary of the strength domain (failure surface), much in the same way as was done by Di Ludovico et al.[33] A specific procedure for the evaluation of the strength domain is not available in OpenSees. Users must therefore apply their skills to develop a method that may serve the purpose, taking advantage of the available procedures. The present authors have used the three following methods.

First method—Given the values of the axial force N and of one bending moment (for example, M_X), the value of the moment M_Y that leads to the ultimate curvature κ_{Yu}—that is, the one derived on the basis of the constitutive model—is obtained via a step-by-step procedure in which the required bending moment is increased gradually until the failure conditions are reached. It should be noticed, however, that the ultimate curvature κ_{Yu} must be provided to terminate the procedure. The authors used the method proposed in the present work to provide the ultimate curvature. In this case, results appear to be fairly good for low and moderately large values of the compression axial force. A maximum error equal to 0.04 is found for an axial force ratio $\nu = 0$ at a moment ratio M_Y/M_X equal to 0.2. Alternatively, the present procedure can be applied by prescribing the axial force N and the bending moment M_Y and by increasing the curvature κ_X up to the ultimate value κ_{Xu} which, as before, has been evaluated by using the method proposed in this work.

The largest error is again equal to 0.04 for an axial force ratio $\nu = 0$, but this time it occurs for a bending moment ratio $M_X/M_Y \cong 0.2$. Although the error incurred by using the procedure described herein is generally rather small, it is clear that there can be instances when it can be noticeable. The results discussed previously were derived by using the OpenSees procedure MomentCurvature3D.tcl.

Second method—Rather than prescribing the axial force N and one bending moment as in the previous method, here, only the axial force N is provided. Then two incremental analyses are performed in sequence; in the first one, the largest between the two curvature components κ_X and κ_Y is increased to the ultimate value $\max\{\kappa_{Xu}, \kappa_{Yu}\}$, while in the second the smallest between the two components is increased to the ultimate value $\min\{\kappa_{Xu}, \kappa_{Yu}\}$.

The results obtained by OpenSees tend to cluster around the axes of the graphs, leaving the central part uncovered, and are not shown for the sake of brevity.

This results in a relatively large error which, in some cases, can reach nearly 0.15 (or 15%) in the region where the two bending moments are almost equal.

One might now wonder why the two incremental analyses were performed in the sequence previously described. As a matter of fact, if this ordering had not been imposed, the succession would have simply been κ_X followed by κ_Y. Very large errors, in the range of 10 to 40%, would have been obtained in most cases. Again, the graphs are not shown for space limitations.

The results referring to the second method described previously were obtained by a simple modification of the example of the OpenSees procedure MomentCurvature3D.tcl.

Third method—In this method, the axial force N is prescribed just as in the two previous methods. The two components κ_{Xu} and κ_{Yu} of the ultimate curvature are assigned together with the prescribed value of the axial force N as a loading condition using the OpenSees Command "sp".

It is important to realize that even in the present case, the method proposed in this work for the evaluation of the ultimate curvature is of paramount importance. The results obtained are shown in the graphs of Fig. 5(a) and in terms of relative error in the graphs of Fig. 5(b).

It is interesting to notice that in this case, the results are similar to those obtained by Di Ludovico et al.,[33] and the relative error is also of the same order of magnitude. A variant of the present method consists in assigning as a loading condition the triplet $\{\varepsilon_G, \kappa_{Xu}, \kappa_{Yu}\}$ corresponding to $\{N, \kappa_{Xu}, \kappa_{Yu}\}$. In this case, the error has been calculated starting from dimensionless expressions of the stress resultants (stress resultant divided by its ultimate value in the absence of the other two). Although the error is almost everywhere below 0.01, there are a few instances where it approaches 0.03. In conclusion, it appears that OpenSees can be advantageously used for the calculation of the strength domain, but the procedure for its calculation should be carefully selected.

From the analyses presented herein, it appears that the third method, where the triplet $\{N, \kappa_{Xu}, \kappa_{Yu}\}$ is prescribed as a load condition, provides the best results, which are also comparable in terms of accuracy with those provided in the literature by using specifically designed procedures. However, the fact that any procedure activated within

OpenSees takes advantage of the method proposed herein should not be overlooked.

This application shows one of the potential uses of the present method which is to check that numerical algorithms for axial force and biaxial bending interaction provide accurate results.

Comparison of results for L cross sections

A series of results concerning an L-shaped section is due to Fafitis.[28] The cross section considered is shown in Fig. 6 and consists of two unequal concrete flanges 21 in. (533.4 mm) thick and 135 in. (3429 mm) and 175 in. (4445 mm) long, respectively. The reinforcement, placed on the centerline, consists of 29#10@10"cc with a design yield stress f_{yd} = 60,000 psi (413.69 MPa). The stated concrete strength is f_{cd} = 9000 psi (62.05 MPa).

The comparison with the results obtained by the present method is given in Fig. 7(a) and the results provided by Fafitis[28] are generally in excellent agreement. As may be seen from Fig. 7(a), the results are provided in the form of graphs M_X-M_Y for three different values of the axial force: N = –9000 kips (–40,034 kN), N = –24,000 kips (–106,757 kN), and N = –44,000 kips (–195,722 kN). At the bottom of the curve corresponding to N = –9000 kips (–40,034 kN); a few of the points provided by Fafitis[28] show a rather erratic behavior. This may indicate that the method used by Fafitis[28] can occasionally have accuracy problems.

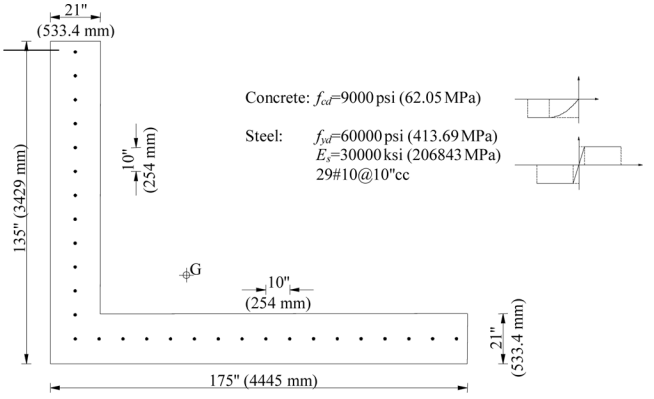

*Fig. 6—*L*-section considered by Fafitis.[28]*

This is confirmed by the relative error curves shown in Fig. 7(b), where a maximum error of nearly 8% is found for an axial force of –9000 kips (–40,034 kN). However, for the remaining values of the axial force considered, the maximum error never exceeds 2%.

The comparison with the results obtained by OpenSees assigning the two limit curvature components and the corresponding limit axial deformation show good agreement, with the relative error never exceeding 0.02.

All of the examples given previously show that the present method is capable of producing the strength domain for any type of reinforced concrete cross section in an efficient way. The way the domain is constructed avoids all problems related to accuracy or convergence in the numerical solution of the nonlinear algebraic equations. The only issues that have to be addressed are the discretization of the boundary of the cross section and the choice of the number of points used for the representation of the boundary surface of the strength domain. The first is, in most cases, not a real issue because the reinforced concrete sections are generally of polygonal form while the second can be easily addressed by increasing the number of points as necessary.

It should be noted that the strength domains obtained by the present method can be replicated by using fiber models in standard computer programs such as OpenSees, provided that a suitable procedure is implemented that accurately simulates the method proposed herein. For instance, the best results with OpenSees are obtained if the limit deformations $\{\varepsilon_G, \kappa_{Xu}, \kappa_{Yu}\}$ are evaluated by the present method and assigned by means of the "sp" command. Slightly better results were found in the authors' comparisons by assigning the alternative triplet $\{N, \kappa_{Xu}, \kappa_{Yu}\}$. However, the first approach should be preferable because in a strength domain, the axial force N is a natural unknown.

Comparison of results for prestressed cross sections

Several results concerning prestressed cross sections have been presented recently by Marmo et al.[40] Although all the cross sections considered by the quoted authors can be easily analyzed by the present method, for the sake of brevity, only the *Y* section shown in Fig. 8 will be discussed herein. The material properties, areas, and positions of the ordinary and prestressing reinforcement they used are not shown herein for the sake of brevity but may be found in Tables 4 through 6 on

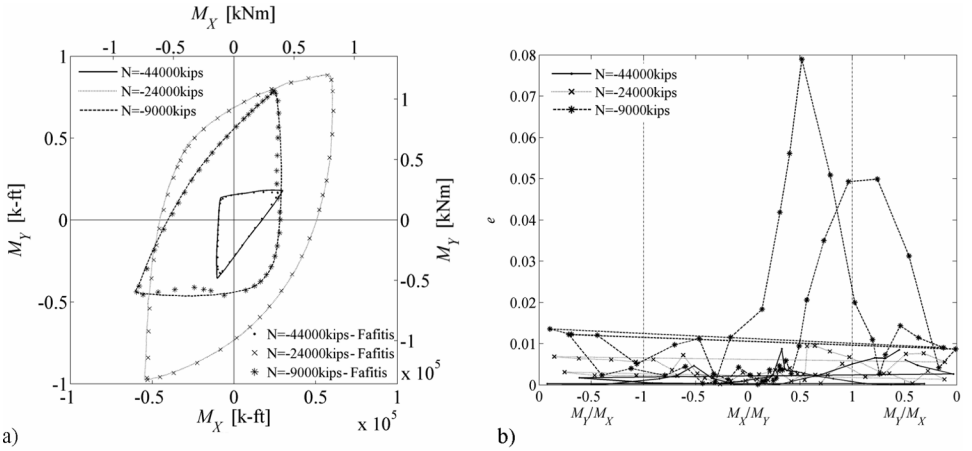

Fig. 7—Cross sections of strength domain for reinforced concrete section of Fig. 6: (a) comparison with results by Fafitis[28]; and (b) relative error.

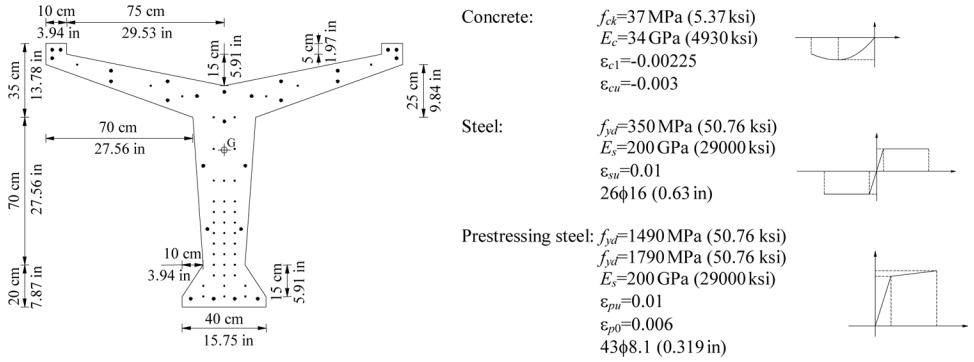

*Fig. 8—*Y*-section considered by Marmo et al.[40]*

page 98 of their paper. Obviously, the strength domain for the considered cross section is a three-dimensional (3-D) surface (Fig. 9), but only the 12 cross sections at constant N given by the authors are shown here to simplify the comparison (Fig. 10). The figure is split into two parts to avoid excessive curve crossing and to maintain each curve as distinctive as possible. The continuous curves refer to the results obtained by the present method while the discrete dots are values provided by the quoted authors. The agreement can be considered good, albeit not perfect, but the limited number of points provided by Marmo et al.[40] is indicative of the minor computational effort required by the present method.

STEEL SECTIONS ENCASED IN CONCRETE

The purpose of this section is twofold. On one hand, it wants to show how the presented method can be used to deal with common technological situations such as steel sections encased in concrete or even tubular steel[41-43] and FRP sections filled with concrete[44]; on the other hand, it wants to show how relevant the appropriateness of the constitutive law for concrete is on the obtained results. To this purpose, a cross section is used (Fig. 11), previously considered by Leon and Hajjar,[42] to illustrate the application of the 2005 AISC Specification. However, in the application presented herein, the specifications of Eurocode 4 for composite steel and concrete structures are used for the material parameters instead of the AISC ones. Eight cross sections of the 3-D strength domain with constant axial force planes are shown with solid lines in Fig. 12. The constitutive law prescribed by Eurocode 4[7] has then been changed by replacing the rectangular part of the stress diagram ($-\alpha f_{cd}$ = –20.68 MPa [–3 ksi]) by a softening branch with ultimate strain $\varepsilon_{cu} = 0.004$ and ultimate stress $\sigma_{cu} = -\beta f_{cd} = -12.7$ MPa (–1.84 ksi). These parameters were evaluated using the Kent and Park[37] law for unconfined concrete. The results are shown with broken lines in Fig. 12 and are significantly different from the previous ones, leading to the conclusion that the constitutive law should be consistent with the application considered. Furthermore, it appears that for tensile axial forces, no significant difference appears between the two constitutive laws if not in the case of bending around the minor axis ($M_X = 0$), due to the fact that the contribution of the encased steel section is less effective. As the compressive axial force becomes larger and larger, the strength domain tends to shrink more and more. Most interesting is the fact that the strength reduction is more pronounced along the principal axes of bending and is minimal along lines of biaxial bending of nearly equal components.

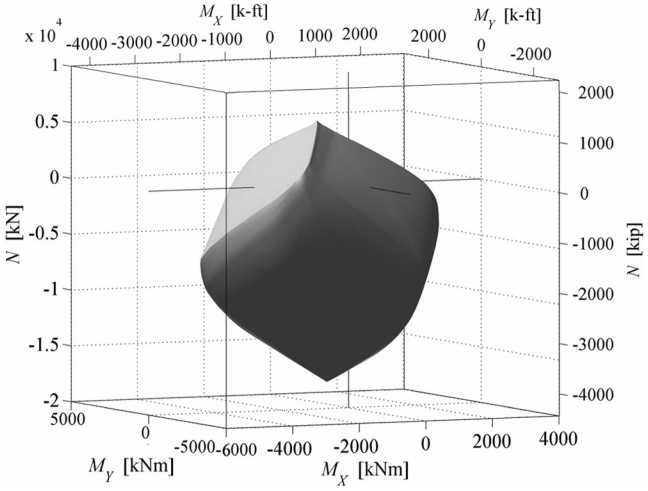

Fig. 9—Three-dimensional strength domain for reinforced concrete section of Fig. 8.

Besides the Kent and Park[37] law for confined concrete, another constitutive law has been formulated for concrete confined by FRP[45,46] and applied to the derivation of strength domains.[47] Such laws and similar ones can be handled efficiently by the present method.

STRENGTH REDUCTION FACTORS AND INSTABILITY EFFECTS

The strength domain constructed with the method described in the previous paragraphs is dependent on the geometry and the material properties of the cross section considered. Its use for design purposes requires modifications that account for different levels of uncertainty associated with failure modes (compression-controlled, intermediate, tensile-controlled) and for local and global geometrical effects related to the member and the structure to which the cross section belongs. Briefly, the different uncertainties related to the failure modes are accounted for, in codes such as ACI 318-08[4] (Chapter 9), by the so-called strength reduction factors, while the geometrical effects are considered via the moment magnifier design procedure (ACI 318-08,[4] Chapter 10). This is a method that enables to account indirectly for geometric nonlinear effects by empirically increasing the bending moments obtained by a linear analysis. This is a difficult and controversial topic because such empirical amplifications could be avoided altogether if member forces were to be determined through a complete material and geometric nonlinear analysis. However, such analyses are usually expensive both in terms

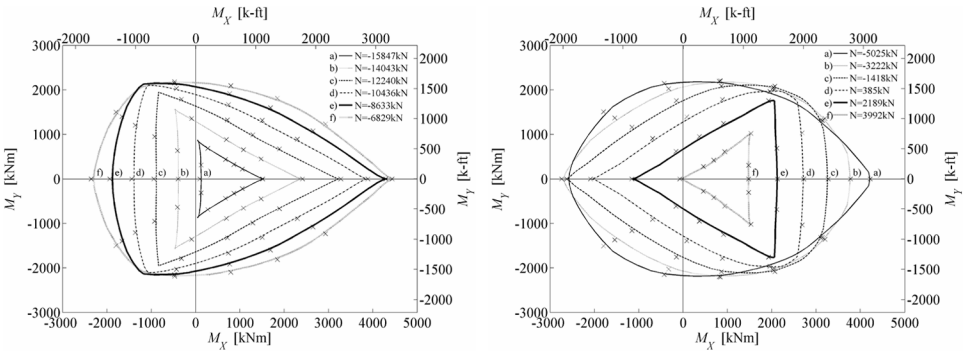

Fig. 10—Cross sections of strength domain for reinforced concrete section of Fig. 8 and comparison with results by Marmo et al.[40]

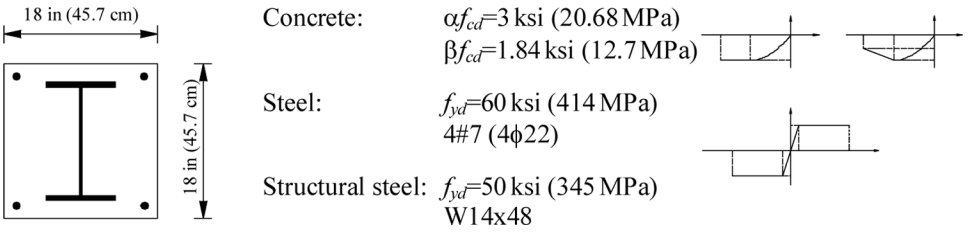

Fig. 11—Reinforced concrete square cross section with embedded W14 x 48 section.

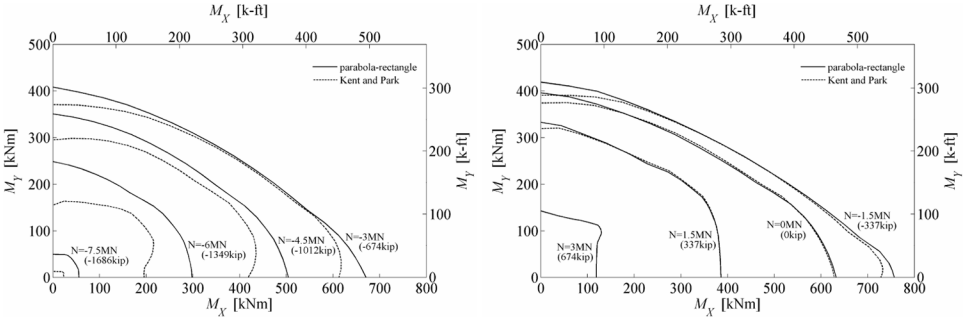

Fig. 12—Cross sections of strength domain for reinforced concrete section of Fig. 11. Comparison between parabola-rectangle constitutive law and Kent and Park[37] constitutive law.

of human expertise and computational effort, making the empirical relations embedded in the codes the most effective and reliable alternative.

CONCLUSIONS

An exact method for the construction of the strength domain of reinforced concrete and of prestressed concrete sections has been presented. The method is direct and does not require iterative procedures. Therefore, it does not exhibit accuracy and convergence problems often shown by methods attempting to solve nonlinear algebraic equations. The strength domain can be used to check the safety conditions of the cross section, especially to see whether code requirements are satisfied. Therefore, it appears to be an extremely useful and simple tool to be used in design. The present method makes the construction extremely simple, quick, and accurate, therefore encouraging its application. If in the design process it is found that one or more loading conditions violate the code requirements, the section must be redesigned with a consequent change of the strength domain; this, however, can be reconstructed with little effort via the present method and the optimal design may be achieved via a trial-and-error procedure.

The strength domain evaluated with the present method has been checked against several results available in the literature. In some cases, the agreement has been excellent; in other cases, the agreement has been generally good, but with some exceptions suggesting numerical problems in the methods used in the literature to derive those results. In a few other cases, the comparison has shown some significant disagreement, probably due to the preliminary nature of the results considered and/or the inappropriate setting of the accuracy and convergence parameters. The present method can be implemented in any software that uses fiber models for the discretization of the cross section. The method can be used efficiently to provide the deformation triplet, which corresponds to a point on the boundary of the strength domain in the stress resultants' space. The evaluation of the corresponding triplet of strength resultants requires only the integration over the cross section of the stresses specified in terms of appropriate constitutive laws from the prescribed limit deformations. This has been applied in the present work by using OpenSees.

REFERENCES

1. Bruneau, M.; Uang, C.; and Whittaker, A., *Ductile Design of Steel Structures*, McGraw-Hill, New York, 1998, 928 pp.

2. Kong, F. K., and Evans, R. K., *Reinforced and Prestressed Concrete*, Van Nostrand Reinhold, UK, 1987, 528 pp.

3. Jirasek, M., and Bažant, Z. P., *Inelastic Analysis of Structures*, John Wiley & Sons, Ltd., New York, 2002, 722 pp.

4. ACI Committee 318, "Building Code Requirements for Structural Concrete (ACI 318-08) and Commentary," American Concrete Institute, Farmington Hills, MI, 2008, 473 pp.

5. AS 3600. "Concrete Structures - AS 3600-2009," Standards Association of Australia, Sydney, Australia, 2009, 213 pp.

6. EN 1992-1-1. "Eurocode 2: Design of Concrete Structures Part 1-1: General—Common Rules for Building and Civil Engineering Structures," European Committee for Standardization, Brussels, Belgium, 2004, 222 pp.

7. EN-1994-1-1. "Eurocode 4: Design of Composite Steel and Concrete Structures Part 1-1: General—Common Rules and Rules for Buildings," European Committee for Standardization, Brussels, Belgium, 2005, 120 pp.

8. EN 1998-1, "Eurocode 8: Design of Structures for Earthquake Resistance Part 1: General Rules, Seismic Actions and Rules for Buildings," European Committee for Standardization, Brussels, Belgium, 2005, 230 pp.

9. Furlong, R. W.; Hsu, C. T. T.; and Mirza, S. A., "Analysis and Design of Concrete Columns for Biaxial Bending—Overview," *ACI Structural Journal*, V. 101, No. 3, May-June 2004, pp. 413-422.

10. Bresler, B., "Design Criteria for Reinforced Concrete Columns under Axial Force and Biaxial Bending," ACI Journal, *Proceedings* V. 57, No. 11, Nov. 1960, pp. 481-490.

11. Ramamurthy, L. N., "Investigation of the Ultimate Strength of Square and Rectangular Columns under Biaxially Eccentric Loads," *Proceedings, Symposium on Reinforced Concrete Columns*, SP-13, American Concrete Institute, Farmington Hills, MI, 1966, pp. 263-298.

12. Ferguson, P. M.; Breen, J. E.; and Jirsa, J. O., *Reinforced Concrete Fundamentals*, fifth edition, John Wiley & Sons, Inc., New York, 1988, 768 pp.

13. Wight, J. K., and MacGregor, J. G., *Reinforced Concrete: Mechanics and Design*, fifth edition, Pearson Prentice Hall, Upper Saddle River, NJ, 2009, 1176 pp.

14. Silva, M. A.; Swan, C. C.; Arora, J. S.; and Brasil, R. M. L. R. F., "Failure Criterion for RC Members under Biaxial Bending and Axial Load," *Journal of Structural Engineering*, ASCE, V. 127, No. 7, 2001, pp. 922-929.

15. Bonet, J. L.; Miguel, P. F.; Fernandez, M. A.; and Romero, M. L., "Analytical Approach to Failure Surfaces in Reinforced Concrete Sections Subjected to Axial Loads," *Journal of Structural Engineering*, ASCE, V. 130, No. 12, 2004, pp. 2006-2015.

16. Park, R., and Paulay, T., *Reinforced Concrete Structures*, Wiley, New York, 1975, 800 pp.

17. Nielsen, M. P., *Limit Analysis and Concrete Plasticity*, CRC Press, New York, 1999, 936 pp.

18. MacGregor, J. G., and Bartlett, F. J., *Reinforced Concrete: Mechanics and Design*, first edition, Prentice-Hall Canada, Scarborough, ON, Canada, 2000, 1041 pp.

19. Kawakami, M. T.; Kagaya, M.; and Hirata, M., "Limit States of Cracking and Ultimate Strength of Arbitrary Cross Sections under Biaxial Loading," ACI Journal, *Proceedings* V. 82, No. 1, Jan.-Feb. 1985, pp. 203-212.

20. Landonio, M., and Perego, R., "Un metodo generale per il calcolo automatico allo stato limite ultimo di sezioni in c.a. soggette a presso flessione deviate," *La prefabbricazione*, V. 2, No. 3, 1986, pp. 112-130.

21. Hulse, R., and Mosley, W. H., *Reinforced Concrete Design by Computer*, Macmillan Education Ltd., New York, 1986, 304 pp.

22. Contaldo, M., and Faella, G., "Un Procedimento per il calcolo Automatico delle Sezioni in c.a," *Giornale del Genio Civile*, V. 10, 1997, pp. 23-37.

23. Spiegel, L., and Limbrunner, G. F., *Reinforced Concrete Design*, Prentice-Hall, Upper Saddle River, NJ, 2002, 506 pp.

24. Bousias, S. N.; Panagiotakos, T. B.; and Fardis, M. N., "Modelling of RC Members under Cyclic Biaxial Flexure and Axial Force," *Journal of Earthquake Engineering*, V. 6, No. 2, 1996, pp. 711-725.

25. De Vivo, L., and Rosati, L., "Ultimate Strength Analysis of Reinforced Concrete Sections Subject to Axial Force and Biaxial Bending," *Computer Methods in Applied Mechanics and Engineering*, V. 166, 1998, pp. 261-287.

26. Rodriguez-Gutierrez, J. A., and Aristizabal-Ochoa, J. D., "Biaxial Interaction Diagrams for Short RC Columns of Any Cross Section," *Journal of Structural Engineering*, ASCE, V. 125, No. 6, 1999, pp. 672-683.

27. Rodriguez-Gutierrez, J. A., and Aristizabal-Ochoa, J. D., "M-P-ϕ Diagrams for Reinforced, Partially, and Fully Prestressed Concrete Sections under Biaxial Bending and Axial Load," *Journal of Structural Engineering*, ASCE, V. 127, No. 6, 2001, pp. 763-773.

28. Fafitis, A., "Interaction Surfaces of Reinforced-Concrete Sections in Biaxial Bending," *Journal of Structural Engineering*, ASCE, V. 127, No. 7, 2001, pp. 840-846.

29. Sfakianakis, M. G., "Biaxial Bending with Axial Force of Reinforced, Composite and Repaired Concrete Sections of Arbitrary Shape by Fiber Model and Computer Graphics," *Advances in Engineering Software*, V. 33, 2002, pp. 227-242.

30. Consolazio, G. R.; Fung, J.; and Ansley, M., "M-Φ-P Diagrams for Concrete Sections under Biaxial Flexure and Axial Compression," *ACI Structural Journal*, V. 101, No. 1, Jan.-Feb. 2004, pp. 114-123.

31. Hock, L. G., and Cheong, F. S., "A Computerized Estimation of Moment-Force Interaction for Externally Strengthened RC Composite Column," *Journal of The Institution of Engineers*, V. 44, No. 1, 2004, pp. 20-38.

32. Charalampakis, A. E., and Koumousis, V. K., "Ultimate Strength Analysis of Arbitrary Cross Sections under Biaxial Bending and Axial Load by Fiber Model and Curvilinear Polygons," *5th GRACM International Congress on Computational Mechanics*, Limassol, Cyprus, June 29-July 1, 2005, 8 pp.

33. Di Ludovico, M.; Lignola, G. P.; Prota, A.; and Cosenza, E., "Analisi non lineare di sezioni in c.a. soggette a pressoflessione deviate," *ANIDIS 2007 XII Convegno Nazionale, L'ingegneria sismica in Italia*, Pisa, Italy, June 10-14, 2007, 12 pp.

34. Bonet, J. L.; Romero, M. L.; Miguel, P. F.; and Fernandez, M. A., "A Fast Stress Integration Algorithm for Reinforced Concrete Sections with Axial Loads and Biaxial Bending," *Computers & Structures*, V. 82, 2004, pp. 213-225.

35. Bonet, J. L.; Barros, M. H. F. M.; and Romero, M. L., "Comparative Study of Analytical and Numerical Algorithms for Designing Reinforced Concrete Sections under Biaxial Bending," *Computers & Structures*, V. 84, 2006, pp. 2184-2193.

36. Marín, J., "Design Aids for L-Shaped Reinforced Concrete Columns," ACI Journal, *Proceedings* V. 76, No. 11, Nov. 1979, pp. 1197-1216.

37. Kent, D. C., and Park, R., "Flexural Members with Confined Concrete," *Journal of the Structural Division*, ASCE, V. 97, No. 7, 1971, pp. 1969-1990.

38. OpenSees: Open System for Earthquake Engineering Simulation, Berkeley, CA, 2009, http://www.opensees.berkeley.edu.

39. Mazzoni, S.; McKenna, F.; Scott, M. H.; Fenves, and G. L. et al., "OpenSees Command Language Manual," Berkeley, CA, 2006, http://www.opensees.berkeley.edu.

40. Marmo, F.; Serpieri, R.; and Luciano, R., "Ultimate Strength Analysis of Prestressed Reinforced Concrete Sections under Axial Force and Biaxial Bending," *Computers & Structures*, V. 89, 2011, pp. 91-108.

41 Leon, R. T.; Kim, D. K.; and Hajjar, J. F., "Limit State Response of Composite Columns and Beam-Columns Part I: Formulation of Design Provisions for the 2005 AISC Specification," *Engineering Journal*, fourth quarter, 2007, pp. 341-358.

42 Leon, R. T., and Hajjar, J. F., "Limit State Response of Composite Columns and Beam-Columns Part II: Application of Design Provisions for the 2005 AISC Specification," *Engineering Journal*, first quarter, 2008, pp. 21-46.

43. Morino, S., and Tsuda, K., "Design and Construction of Concrete-Filled Steel Tube Column System in Japan," *Earthquake Engineering and Engineering Seismology*, V. 4, No. 1, 2003, pp. 51-73.

44. Mohamed, H., and Masmoudi, R., "Behavior of FRP Tubes-Encased Concrete Columns under Concentric and Eccentric Loads," *Composites & Polycon*, American Composites Manufacturers Association, Jan. 15-17, 2009, 8 pp.

45. Pellegrino, C., and Modena, C., "Analytical Model for FRP Confinement of Concrete Columns with and without Internal Steel Reinforcement," *Journal of Composites for Construction*, V. 14, No. 6, 2010, pp. 693-705.

46. Lam, L., and Teng, J. G., "Design-Oriented Stress-Strain Model for FRP-Confined Concrete," *Construction & Building Materials*, V. 17, No. 6-7, 2003, pp. 471-489.

47. Rocca, S.; Galati, N.; and Nanni, A., "Interaction Diagram Methodology for Design of FRP-Confined Reinforced Concrete Columns," *Construction and Building Materials*, V. 23, 2009, pp. 1508-1520.